IEEE Access
Multidisciplinary | Rapid Review | Open Access Journal

Received June 9, 2020, accepted July 2, 2020, date of publication July 10, 2020, date of current version July 27, 2020.

Digital Object Identifier 10.1109/ACCESS.2020.3008480

A Method for the Micro-Motion Signal Separation and Micro-Doppler Extraction for the Space Precession Target

XUGUANG XU[1], CUNQIAN FENG[2], AND SISAN HE[2]
[1]Graduate College, Air Force Engineering University, Xi'an 710051, China
[2]Air and Missile Defense College, Air Force Engineering University, Xi'an 710051, China

Corresponding author: Xuguang Xu (xuxuguanghjbsqsbs@163.com)

This work was supported by the National Natural Science Foundation of China under Grant 61701528.

ABSTRACT Aiming at the problem of micro-motion signal separation and micro-Doppler extraction of the precession target, a new method based on singular value decomposition (SVD) and joint approximate diagonalization of eigen-matrices (JADE) is proposed in this paper. Firstly, the micro-motion model of space precession target is established, and the micro-Doppler and scattering characteristics are analyzed to establish the echo signal model of the target. Secondly, through simplifying the signal model of scattering point and building the signal matrix of different signal lengths, the singular value ratio sequence is constructed by the method of SVD to estimate the precession period of the target. Thirdly, the singular vectors of different observation periods are extracted, the observation matrix is constructed, and then the JADE algorithm is adopted to separate the micro-motion signal of each scattering point. Finally, the clustering analysis is used to denoise the time-frequency graph and the centroid calculation is employed to extract the micro-Doppler of each scattering point. Simulation results show that this method of good robustness can effectively separate and extract the micro-Doppler of the scattering points.

INDEX TERMS Micro-motion, singular value decomposition, joint approximate diagonalization of eigen-matrices, micro-Doppler extraction.

I. INTRODUCTION

In recent years, with the attention of various countries in the field of space safety, space target detection and recognition technology has become the focus of current researches [1]–[3]. When the target is flying in space, it is necessary to spin to keep flight attitude and reentry angle stable [4]. Meanwhile, when the target releases other flying objects, it will be disturbed by the lateral torque, thus the precession of the target will be formed. V. C. Chen defines the concept of micro-motion of the target, which is different from the motion of the main body, including spinning, conning, swing and precession [5]. Through the analysis and research of the micro-motion state of the target, the characteristics of the target can be revealed effectively and good foundations for the recognition of space targets are laid [6]–[8]. As a result, the research on micro-motion arouses the widespread concern of scholars all over the world.

The associate editor coordinating the review of this manuscript and approving it for publication was Byung-Gyu Kim.

According to the scattering characteristics of the target in the optical zone, the echo of the target can be represented as the sum of echoes from several local strong scattering points [9]. Also, there is almost no mutual influence between the echoes of the scattering points. As a result, the micro-motion information is superimposed in time domain, frequency domain and time-frequency domain, which leads to the difficulty and complexity of micro-motion signal separation. Accordingly, in the process of analyzing the micro-motion characteristics of the target, it is one of the most important steps to separate the micro-motion signal belonging to each scattering point.

As a significant micro-motion information, micro-Doppler plays an important role in the analysis of micro-motion target characteristics. As for the problem of extracting the micro-Doppler of scattering points, many scholars have carried out researches in this area and obtained significant results. Chen used maxima extraction algorithm to extract the micro-Doppler of single component signal from the time-frequency graph [10]. Zhou applied the Hough

transform to separate the micro-motion signal and estimate the micro-Doppler parameters [11]. Sathe adopted the Inverse Radon Transform (IRT) to estimate the micro-motion parameters of the helicopter main and tail rotor blades [12]. Han proposed a micro-Doppler association algorithm for the multi scattering points by employing Kalman filter and target tracking theory to associate the time-micro-Doppler curve of different scattering points [13]. Li presented a micro-Doppler extraction algorithm, Viterbi algorithm, based on the energy information of time-frequency graph, but this algorithm was easily affected by noise and its robustness was bad [14]. In order to overcome the association errors at the time-frequency intersection in [14], Li proposed an improved Viterbi algorithm, in which the micro-Doppler change rate was added to the penalty function [15]. D. P. Fairchild extracted human micro-Doppler signatures of different movements by adopted the empirical mode decomposition [16]. Djokovic employed the short-time Fourier transform to estimate the parameters roughly in the first stage and refined the micro-Doppler parameters in the second stage [17]. Vishwakarma established the micro-Doppler feature model with dictionary learning and used the sparse coding algorithm to separate the scattering point from the group targets [18].

The above researches on micro-motion separation and micro-Doppler extraction mainly have the following shortcomings: some methods rely too much on signal models and have limited scope of application; the separation and extraction are mostly performed in time-frequency domain and are at the same time, which is easy to cause extraction errors at the time-frequency intersection. To overcome the above shortcomings, a micro-motion signal separation and micro-Doppler extraction method based on SVD and JADE is proposed. Based on the periodicity of the precession target, the signal matrices under different signal lengths are constructed and then decomposed by SVD. Also, the singular value ratio sequence for which the period of the target is estimated by peak search. After the estimation, the eigenvectors corresponding to the maximum singular values and the basic signals with different amplitude coefficients are obtained, the observation matrix is constructed, and then the basic signal of each scattering point is separated by JADE. As for the separated signals, the clustering analysis is adopted to denoise the time-frequency graph and the centroid calculation is employed to extract the micro-Doppler. Finally, simulation experiments are conducted to verify the effectiveness of the proposed method.

The rest of this paper is organized as follows. Section II establishes the micro-motion model and the signal model. In Section III, the algorithm of precession period estimation based on SVD, the separation of the micro-motion signal based on JADE and the extraction of the micro-Doppler are presented. Performance analysis of the proposed method is conducted through simulation in Section IV. Section V is the conclusion.

II. MODEL OF CONE-SHAPED SPACE PRECESSION TARGET

The motion of the space precession target consists of two parts: orbital motion and precession. On one hand, the orbital motion changes the radar observation angle of the target, which will further change the scattering coefficients. On the other hand, the orbital motion will result in Doppler superimposed on the micro-Doppler, which is not conducive to the extraction of micro-Doppler. In this paper, the change of the scattering coefficients is useful for the signal separation so that it is taken into consideration. On the contrary, the orbital motion is not conducive to the micro-Doppler extraction, so it needs to be compensated.

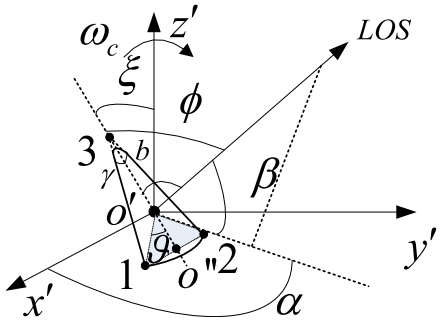

FIGURE 1. Precession model of the cone-shaped target.

A. PRECESSION MODEL OF THE TARGET

The precession model of the cone-shaped target is shown in Fig. 1. Set z' as the precession axis, the intersection point o' of the target symmetry axis and the precession axis as the coordinate origin, and the reference coordinate system $o'x'y'z'$ is set up. Set LOS as the radar line of sight, α as the azimuth angle of LOS, β as the pitch angle of LOS, $\phi(t)$ as the angle between the radar line of sight and the target symmetry axis, ξ as the angle between the target symmetry axis and z'. Set the cone top scattering point as scatter 3, the two sliding scattering points as scatter 2 and scatter 1. Set o'' as the center of the bottom of the conical warhead, γ as the half cone angle, ϑ as the angle between $o'o''$ and the line from o' to scatter1. Set a as the radius of the bottom circle, b as the top radius. The length from o' to scatter1 is h_1, the length from o' to scatter2 is l, and the length of $o'o''$ is h_2. Considering that the cone-shaped target is rotationally symmetrical, the influence of spinning on micro-range of the target will not be reflected in the echo. Therefore, only the influence of the conning on the target is considered. The conning frequency is set as ω_c, and the period corresponding to ω_c is T_c.

Set $\boldsymbol{\eta}$ as the unit vector of the LOS, and it can be expressed as

$$\boldsymbol{\eta} = [\cos\alpha\cos\beta, \sin\alpha\cos\beta, \sin\beta]^T \tag{1}$$

In order to simplify the problem, the symmetry axis of the target is supposed to be in the plane YOZ when $t = 0$. Set $\mathbf{e}$ as the unit vector of the symmetry axis, and it is

expressed as

$$\mathbf{e} = [\sin\xi, 0, \cos\xi]^T \tag{2}$$

When the target conducts precession, the unit vector will change with time. Set $\mathbf{e_d}$ as the unit vector of the symmetry axis, and it is written as

$$\mathbf{e_d} = [\sin\xi\cos(\omega_c t), \sin\xi\sin(\omega_c t), \cos\xi]^T \tag{3}$$

According to (1), (2) and (3), the angle between the radar line of sight and the target symmetry axis satisfies the following equation.

$$\begin{aligned}\cos(\phi(t)) &= \boldsymbol{\eta}\times\mathbf{e_d}\\ &= \sin\xi\cos\beta\sin(\omega_c t+\alpha)+\cos\xi\sin\beta\end{aligned} \tag{4}$$

Set R_{md} as the micro-range. The micro-range of each scattering point can be expressed as

$$\begin{cases} R_{md-3} = h_1\cos(\phi(t)) \\ R_{md-1/2} = h_2\cos(\phi(t)) \pm r\sin(\phi(t)) \end{cases} \tag{5}$$

Set f_{md} as the micro-Doppler. The relationship between f_{md} and R_{md} is represented as

$$f_{md} = \frac{2}{\lambda}\frac{dR_{md}}{dt} \tag{6}$$

where λ denotes the wavelength of the radar. According to (4), (5) and (6), the micro-Doppler of each scattering point is derived as

$$\begin{cases} f_{md-3} = \dfrac{2h_1}{\lambda}\sin\xi\cos\beta\omega_c\cos(\omega_c t+\alpha) \\ f_{md-1/2} = \dfrac{2l\omega_c\sin\xi\cos\beta\cos(\omega_c t+\alpha)}{\lambda} \\ \qquad\times[\cos\vartheta \mp \dfrac{2\cos\phi(t)}{\sqrt{1-\cos^2\phi(t)}}] \end{cases} \tag{7}$$

We can draw the conclusion from (7): the micro-Doppler is determined by multiple parameters, such as the observation angle (α and β), the target physical structure (h_1 and l) and so on, which makes the micro-Doppler difficult to be extracted based on the traditional parameterized extraction methods.

B. SIGNAL MODEL OF THE TARGET

According to [19], the scattering coefficients will change with the flying attitude of the target. Those three scattering coefficients σ_1, σ_2 and σ_3 of the cone-shaped target in Fig. 1 are given as

$$\sigma_1 = \sigma_0\left[e^{-1} \mp \left(e+1-\cos\frac{3\pi-2\phi(t)}{n}\right)^{-1}\right] \tag{8}$$

$$\sigma_2 = \begin{cases} \sigma_0\left[\dfrac{1}{e} \mp \left(e+1-\cos\dfrac{3\pi+2\phi(t)}{n}\right)^{-1}\right] & 0 < \phi(t) < \gamma \\ 0 & \gamma < \phi(t) < \dfrac{\pi}{2} \\ \sigma_0\left[\dfrac{1}{e} \mp \left(e+1-\cos\dfrac{\pi-\phi(t)}{n}\right)^{-1}\right] & \dfrac{\pi}{2} \le \phi(t) \end{cases} \tag{9}$$

$$\sigma_3 = \begin{cases} \sqrt{\pi b}\left[1-\dfrac{\sin[2k_0 b(1-\sin\gamma)]}{k_0 b\cos^2\gamma}^{-1/2}\right] & 0 = \phi(t) \\ \sqrt{\pi b} & 0 < \phi(t) < \dfrac{\pi}{2}-\gamma \\ 0 & \phi(t) \ge \dfrac{\pi}{2}-\gamma \end{cases} \tag{10}$$

where $n = 1.5+\gamma/\pi$, $k_0 = 2\pi\frac{f_c}{c}$, f_c represents the frequency of the radar, and c denotes the speed of the light. σ_0 and e are shown as

$$\begin{cases} \sigma_0 = \dfrac{\sin(\pi/n)}{n}\sqrt{\dfrac{a}{k_0\sin\phi(t)}} \\ e = \cos\dfrac{\pi}{n}-1 \end{cases} \tag{11}$$

It can be seen from (8)-(11) that the scattering coefficients are mainly related to $\phi(t)$. As the target moves in space, the scattering coefficients also shows distinct time-varying characteristics. In this paper, the time-varying characteristic of scattering coefficient is utilized to separate the micro-motion signal of each scattering point.

For the reason that the orbital motion is not conductive to the micro-Doppler extraction, it needs to be compensated. Thus, the method proposed in [20] is employed to compensate the orbital motion. The estimation of precession period is a prerequisite for the realization of orbital motion compensation method in [20]. In [21], the circular correlation coefficients were adopted to estimate the micro-motion period of signal when the micro-motion was accompanied by translational motion. In [22], Zhang introduced the concentration statistics of ambiguity function to estimate the micro-Doppler period when the micro-motion and orbital motion existed at the same time. Actually, we could adopt the algorithm based on the high-order ambiguity function to estimate the precession period [22]. Considering that the orbital motion compensation is not the focus of this paper, the details are not described here.

Therefore, only the effect of the micro-range on the phase of the echo should be considered. As a result, the target echo signal is modeled as

$$\begin{aligned} s(t) &= \left(\sum_{i=1}^{M} s_i(t)\right) + v(t) \\ &= \left(\sum_{i=1}^{M}\sigma_i\exp(j\frac{4\pi f_c(R_{md-i}-R_0)}{c})\right) + v(t) \end{aligned} \tag{12}$$

where M is the number of the scattering point, R_0 is the distance from the target to radar when $t = 0$, R_{md-i} is the micro-range of the ith scattering point, and $v(t)$ is the Gaussian white noise.

III. MICRO-MOTION SIGNAL SEPARATION AND MICRO-DOPPLER EXTRACTION

A. PRECESSION PERIOD ESTIMATION

It can be seen from (4) and (7) that the phase change of the scattering points of the precession target is periodical.

As such, it is necessary to estimate the precession period of the target firstly. In this paper, the period is estimated by the singular value ratio sequence of the signal matrices with different lengths.

In order to further illustrate the problem, it needs to simplify the model of $s(t)$. According to (4), $\phi(t)$ is approximately in a sinusoidal form, and its amplitude is determined only by the initial observation angle. The orbital motion flight duration is probably hundreds of seconds while the precession period is always less than one second. Therefore, this paper assumes that the radar observation angle remains unchanged in current period and changes slightly in the next period. Correspondingly, the angle between the radar line of sight and the cone axis changes from $\phi(t)$ to $\phi(t)+\Delta$ when the time changes from t to $t+T_c$. It is found that Δ is close to 10^{-4}rad, which will have less effect on the micro-Doppler of the target.

According to (8) (9) and (11), it can be seen that 2π rad is much larger than Δ, so that the change of $\frac{3\pi-2\phi(t)}{n}$, $\frac{3\pi+2\phi(t)}{n}$ and $\frac{\pi-\phi(t)}{n}$ in (8) and (9) can be ignored when the time changes from t to $t+T_c$. Therefore, the influence of Δ on scattering coefficient is mainly reflected in $\sqrt{\frac{a}{k_0\sin\phi(t)}}$. In short-term observation, the ratio of σ in adjacent periods can be approximated to

$$\frac{\sigma(t+T_c)}{\sigma(t)} \propto \frac{\sin(\phi(t)+\Delta)}{\sin(\phi(t))} \tag{13}$$

Taking the value of Δ which is close to 10^{-4}rad into consideration, we can draw the conclusion in (14).

$$\lim_{\Delta\to 0}\frac{\sin(\phi(t)+\Delta)}{\sin(\phi(t))} \approx 1+\Delta \tag{14}$$

Therefore, the signal of the scattering point can be further simplified. In the lth period, the echo of ith the scattering point $s_{l,i}(t)$ is given as

$$s_{l,i}(t) = \lambda_{l,i}H_i(t) \tag{15}$$

where $\lambda_{l,i}$ denotes the amplitude modulation coefficient of the signal in the lth period and are different in different periods. $H_i(t)$ represents the basic signal, in which the micro-Doppler information is hidden. The method presented in this paper is to obtain several $H_i(t)$ with different amplitude coefficients and thence the micro-motion signals can be separated.

Set N as the length of the signal. We divide the signal $s(t)$ in (12) into N_c parts, and the length of each part is N_r. The signal matrix $\mathbf{S}$ can be defined as

$$\mathbf{S} = \left[s_{N_r,1}\ s_{N_r,2}\ \cdots\ s_{N_r,N_c} \right]^H \tag{16}$$

where $(\cdot)^H$ represents that the matrix is processed by conjugate transpose. The relationship between N_r and N_c can be expressed as

$$N_c = \mathrm{floor}(\frac{N}{N_r}) \tag{17}$$

where floor(X) rounds X to the nearest integer less than or equal to that element. Theoretically, the range of N_r is [1 N]. In fact, the range of N_r can be chosen according to the range of the precession period.

Singular value decomposition (SVD) is an important method in matrix analysis, which can effectively reveal the internal structure of the matrix and highlight the characteristics of the matrix [23]. The SVD of the matrix $\mathbf{G}$ can be expressed as

$$\mathbf{G} = \mathbf{U}\Lambda\mathbf{V}^H \tag{18}$$

where $\mathbf{U}$ is called the left singular matrix, and $\mathbf{V}$ is called the right singular matrix. The elements on the diagonal of $\mathbf{\Lambda}$ represent the square of the eigenvalue of $\mathbf{G}^H\mathbf{G}$, $\mathbf{\Lambda}$ is given as

$$\mathbf{\Sigma} = \mathrm{diag}(\mu_1, \mu_2, \cdots \mu_r, 0, \cdots, 0) \tag{19}$$

where $r = rank(\mathbf{G})$, $\mu_1 \geq \mu_2 \geq \cdots \geq \mu_r$, and the column vector in $\mathbf{V}$ is the eigenvector corresponding to the singular value in $\mathbf{\Lambda}$. In addition, when $\mathbf{G} = \sum_{q=1}^{Q}\mathbf{G}_q$ and $\mathbf{G}_q^H\mathbf{G}_q$ is an Hermite matrix, $\mathbf{\Sigma}$ can be rewritten as

$$\begin{aligned}\mathbf{\Lambda} &= \sum_{q=1}^{Q}\mathbf{\Lambda}_q \\ &= \sum_{q=1}^{Q}\mathrm{diag}(\mu_1^q, \mu_2^q, \cdots \mu_{r_q}^q, 0, \cdots, 0)\end{aligned} \tag{20}$$

where $r_q = rank(\mathbf{G}_q)$, $\mu_{r_q}^q$ is the r_qth eigenvalue of $\mathbf{G}_q^H\mathbf{G}_q$.

In order to reveal the characteristic of $\mathbf{S}$, set $\mathbf{G} = \mathbf{S}$, and $\mathbf{S}^H\mathbf{S}$ is derived as

$$\begin{aligned}\mathbf{S}^H\mathbf{S} &= \left[s_{N_r,1} \quad s_{N_r,2} \quad \cdots \quad s_{N_r,N_c} \right] \\ &\quad \times \left[s_{N_r,1} \quad s_{N_r,2} \quad \cdots \quad s_{N_r,N_c} \right]^H \\ &= s_{N_r,1} \times s_{N_r,1}^H + \cdots + s_{N_r,N_c} \times s_{N_r,N_c}^H \\ &= \sum_{j=1}^{N_c}\left[s_{N_r,j} \times s_{N_r,j}^H \right] \\ &= \sum_{j=1}^{N_c}\left[\left([\sum_{i=1}^{M} s_{N_r,j,i}(t)] + v_{Nr,j}(t) \right) \right. \\ &\quad \left. \times \left([\sum_{i=1}^{M} s_{N_r,j,i}(t)] + v_{Nr,j}(t) \right)^H \right] \\ &= \sum_{j=1}^{N_c}\left[\sum_{i=1}^{M}\left(s_{N_r,j,i}(t) \times s_{N_r,j,i}(t)^H \right) \right] \\ &\quad + \sum_{j=1}^{N_c}\left[\sum_{i=1}^{M}\left(s_{N_r,j,i}(t) \times [\sum_{l=1,l\neq i}^{M} s_{N_r,j,l}(t)^H] \right) \right] \\ &\quad + \sum_{j=1}^{N_c}\left[[\sum_{i=1}^{M} s_{N_r,j,i}(t)] \times v_{Nr,j}(t)^H \right]\end{aligned}$$

$$+\sum_{j=1}^{N_c}\left[v_{Nr,j}(t)\times[\sum_{i=1}^{M}s_{N_r,j,i}(t)^H]\right]$$
$$+\sum_{j=1}^{N_c}\left[v_{Nr,j}(t)\times v_{Nr,j}(t)^H\right] \quad (21)$$

As for the precession target in Fig. 1, the signals belonging to different scattering points are independent and uncorrelated [24].

Define two random time series, z_1 and z_2. Set $\mathbf{R}$ as the correlation matrix. $\mathbf{R}$ is given as

$$\mathbf{R}=z_1\times z_2^H \quad (22)$$

According to the theory of random signal processing, if z_1 and z_2 are not related and the length of z_1 and z_2 is long enough, $\mathbf{R}$ tends to be a zero matrix [25].

Apply the above theory in (22) to (21), and (21) can be rewritten as

$$\begin{aligned}\mathbf{S}^H\mathbf{S}&\approx\sum_{j=1}^{N_c}\sum_{i=1}^{M}\left(s_{N_r,j,i}(t)\times s_{N_r,j,i}(t)^H\right)\\&\quad+\sum_{j=1}^{N_c}\left(v_{Nr,j}(t)\times v_{Nr,j}(t)^H\right)\\&=\sum_{i=1}^{M}\sum_{i=1}^{N_c}\left(s_{N_r,j,i}(t)\times s_{N_r,j,i}(t)^H\right)+N_c\delta_v^2\mathbf{I}\\&=\left(\sum_{i=1}^{M}\mathbf{R}_{N_r,i}\right)+N_c\delta_v^2\mathbf{I}\end{aligned} \quad (23)$$

where $\mathbf{R}_{N_r,i}$ is the autocorrelation matrix of the ith scattering point, and δ_v^2 is variance of the noise.

Set T_c as the precession period, N_T as the length of the echo in one period. $N_T=PRF\times T_c$, where PRF denotes the pulse repetition frequency.

The ratio of the maximum singular value to other singular values at N_r can be used as an indicator to determine whether N_r is the length of the period. According to the actual value range of N_r, calculate the minimum value of N_c by (17) and set $N_e=\min(N_c)$. Set ρ_{N_r} as the indicator when the segment length is N_r, and the expression of ρ_{N_r} is as

$$\rho_{N_r}=\frac{u_{1,N_r}}{u_{N_e,N_r}} \quad (24)$$

where u_{1,N_r} is the biggest singular value when the segment length is N_r. u_{N_e,N_r} is the N_eth singular value when the segment length is N_r.

According to [26], when $N_r=kN_T, k\in[1,2,3\cdots]$, all the $\mathbf{R}_i$ will be a strictly rank-one matrix and all the singular value will be zero except μ_1^q, which means the singular values of $\mathbf{S}^H\mathbf{S}$ are $\sqrt{N_c\delta_v^2}$ except $u_{1,N_r}=\sqrt{\left[\left(\sum_{i=1}^{M}u_1^i\right)+N_c\delta_v^2\right]}$ and ρ_{N_r} will be very large. When $N_r\neq kN_T, k\in[1,2,3\cdots]$, the rank of $\mathbf{R}_i$ will be N_c and ρ_{N_r} will decrease sharply to a relatively small value. That means ρ_{N_r} will exhibit repeating peaks for different N_r when N_r is multiple of N_T.

Calculate all the ρ_{N_r} and construct the singular value ratio sequence. After peak search of ρ_{N_r}, the precession period of the target will be estimated.

B. MICRO-MOTION SIGNAL SEPARATION

The singular value characteristics of the $\mathbf{S}$ are analyzed above. Next, we analyze the characteristic of the singular vectors.

Set $s_{N_r,i}(t)$ as the echo of the ith scattering point when $N_r=kN_T, k\in[1,2,3\cdots]$. According to (15), $s_{N_r,i}(t)$ is given as

$$s_{N_r,i}(t)=\begin{bmatrix}\lambda_{1,i}H_i\\\lambda_{2,i}H_i\\\vdots\\\lambda_{k,i}H_i\end{bmatrix} \quad (25)$$

Construct the signal matrix $\mathbf{S}$ and $\mathbf{S}^H\mathbf{S}$ can be derived as

$$\begin{aligned}&\mathbf{S}^H\mathbf{S}\\&\approx\lim_{N_r\to\infty}\left\{\sum_{j=1}^{N_c}\left[\left(\sum_{i=1}^{M}s_{N_r,j,i}(t)\right)\times\left(\sum_{p=1}^{M}s_{N_r,j,p}(t)^H\right)\right]+N_c\delta_v^2\mathbf{I}\right\}\\&=\sum_{j=1}^{Nc}\left\{\left[\sum_{i=1}^{M}\lambda_{1,i}H_i,\ \sum_{i=1}^{M}\lambda_{2,i}H_i,\ \cdots,\ \sum_{i=1}^{M}\lambda_{k,i}H_i\right]\times\left[\sum_{i=1}^{M}\lambda_{1,i}H_i,\ \sum_{i=1}^{M}\lambda_{2,i}H_i,\ \cdots,\ \sum_{i=1}^{M}\lambda_{k,i}H_i\right]^H\right\}+N_c\delta_v^2\mathbf{I}\\&=\begin{bmatrix}\sum_{i=1}^{M}\sum_{p=1}^{M}c_{i,p,1,1}H_iH_p^H,&\cdots,&\sum_{i=1}^{M}\sum_{p=1}^{M}c_{i,p,1,k}H_iH_p^H\\\vdots&\ddots&\vdots\\\sum_{i=1}^{M}\sum_{p=1}^{M}c_{i,p,k,1}H_iH_p^H,&\cdots,&\sum_{i=1}^{M}\sum_{p=1}^{M}c_{i,p,k,k}H_iH_p^H\end{bmatrix}+N_c\delta_v^2\mathbf{I}\end{aligned} \quad (26)$$

where $c_{i,p,\cdot,\cdot}$ denotes the amplitude coefficient of the correlation matrix of different basic signals at different observation times and all of them are positive.

According to the mentioned assumption above, when $N_r=kN_T, k\in[1,2,3\cdots]$, there are two cases of the eigenvalues of $\mathbf{S}^H\mathbf{S}$: the maximum is equal to $\left(\sum_{i=1}^{M}u_1^i\right)+N_c\delta_v^2$ and others are equal to $N_c\delta_v^2$. Set g_1 and g_2 as the eigenvectors corresponding to these two eigenvalues.

After careful observation and analysis of $\mathbf{S}^H\mathbf{S}$, we suppose the expression of g_1 is shown in (27).

$$g_1 = \begin{bmatrix} \sum_{i=1}^{M} w_{1,i}H_i \\ \sum_{i=1}^{M} w_{2,i}H_i \\ \vdots \\ \sum_{i=1}^{M} w_{k,i}H_i \end{bmatrix} = \left[\sum_{i=1}^{M} w_{1,i}H_i^T, \sum_{i=1}^{M} w_{2,i}H_i^T, \cdots, \sum_{i=1}^{M} w_{k,i}H_i^T\right]^T \quad (27)$$

Perform $\mathbf{S}^H\mathbf{S} \times g_1$ and the result is shown in (28).

$$\begin{aligned}
&\mathbf{S}^H\mathbf{S} \times g_1 \\
&= \begin{bmatrix} \sum_{i=1}^{M}\sum_{p=1}^{M} c_{i,p,1,1}H_iH_p^H, & \cdots, & \sum_{i=1}^{M}\sum_{p=1}^{M} c_{i,p,1,k}H_iH_p^H \\ \vdots & \ddots & \vdots \\ \sum_{i=1}^{M}\sum_{p=1}^{M} c_{i,p,k,1}H_iH_p^H, & \cdots, & \sum_{i=1}^{M}\sum_{p=1}^{M} c_{i,p,k,k}H_iH_p^H \end{bmatrix} \\
&\quad \times \begin{bmatrix} \sum_{i=1}^{M} w_{1,i}H_i \\ \sum_{i=1}^{M} w_{2,i}H_i \\ \vdots \\ \sum_{i=1}^{M} w_{k,i}H_i \end{bmatrix} \\
&\quad + N_c\delta_v^2\mathbf{I} \times \left[\sum_{i=1}^{M} w_{1,i}H_i^T, \sum_{i=1}^{M} w_{2,i}H_i^T, \cdots, \sum_{i=1}^{M} w_{k,i}H_i^T\right]^T \\
&= \left[\sum_{i=1}^{M} w'_{1,i}H_i^T, \sum_{i=1}^{M} w'_{2,i}H_i^T, \cdots, \sum_{i=1}^{M} w'_{k,i}H_i^T\right]^T \\
&\quad + N_c\delta_v^2 \left[\sum_{i=1}^{M} w'_{1,i}H_i^T, \sum_{i=1}^{M} w'_{2,i}H_i^T, \cdots, \sum_{i=1}^{M} w'_{k,i}H_i^T\right]^T \\
&= \rho \left[\sum_{i=1}^{M} w'_{1,i}H_i^T, \sum_{i=1}^{M} w'_{2,i}H_i^T, \cdots, \sum_{i=1}^{M} w'_{k,i}H_i^T\right]^T \\
&= \rho g_1
\end{aligned} \quad (28)$$

Obviously, ρ is the eigenvalue of $\mathbf{S}^H\mathbf{S}$ which is larger than $N_c\delta_v^2$, and g_1 is the corresponding eigenvector. Therefore, we treat g_1 as the eigenvector corresponding to the largest singular value u_{1,N_r} when $N_r = kN_T, k \in [1, 2, 3\cdots]$.

When the eigenvalue is $N_c\delta_v^2$, g_2 satisfies the following relationship equation,

$$\mathbf{S}^H\mathbf{S} \times g_2 = N_c\delta_v^2 g_2 \quad (29)$$

Bring (29) into (26), and (29) can be simplified to (30),

$$\begin{bmatrix} \sum_{i=1}^{M}\sum_{p=1}^{M} c_{i,p,1,1}H_iH_p^H, & \cdots, & \sum_{i=1}^{M}\sum_{p=1}^{M} c_{i,p,1,N_c}H_iH_p^H \\ \vdots & \ddots & \vdots \\ \sum_{i=1}^{M}\sum_{p=1}^{M} c_{i,p,N_c,1}H_iH_p^H, & \cdots, & \sum_{i=1}^{M}\sum_{p=1}^{M} c_{i,p,N_c,N_c}H_iH_p^H \end{bmatrix} g_2 = 0 \quad (30)$$

Set the expression of g_2 as the following equation,

$$g_2 = [h_1^T, h_2^T, \cdots, h_{Nc}^T]^T \quad (31)$$

For the reason that all $c_{i,p,.,.}$ are positive, we draw the conclusion in (32),

$$\begin{cases} h_1 \perp H_i \\ h_2 \perp H_i \\ \vdots \\ h_{N_c} \perp H_i \end{cases} \quad i = 1, 2, \cdots M \quad (32)$$

where $\perp$ represents those two vectors are orthogonal. From (31) and (32), we know that $g_2 \perp g_1$.

Comparing (25) with (27), it can be found that only the amplitude coefficients are different but the basic signal H_i is contained in both g_1 and $s_{N_r,i}(t)$, which means that the micro-Doppler information keeps unchanged.

According to singular value decomposition theory [23], g_1 and g_2 are the eigenvectors of $\mathbf{S}^H\mathbf{S}$ and also the singular vectors of $\mathbf{S}$. g_1 is the singular vector corresponding to the largest singular value, so it is located in the first column of $\mathbf{V}$. As such, g_1 can be extracted from $\mathbf{V}$ when it is needed.

Set K as the number of the observation signal, and the value of k is K. Set $N_r = K \times N_T$. Construct the signal matrix $\mathbf{S}$, perform SVD on $\mathbf{S}$ and extract the eigenvector g^K corresponding to the largest singular value.

$$g^K = \left[\sum_{i=1}^{M} w_{1,i}H_i^T, \sum_{i=1}^{M} w_{2,i}H_i^T, \cdots, \sum_{i=1}^{M} w_{k,i}H_i^T\right]^T \quad (33)$$

Divide g^K into K segments and the length of each segment is N_T. Arrange these segments into an observation matrix $\mathbf{Y}$. $\mathbf{Y}$ can be written as

$$\begin{aligned}
\mathbf{Y} &= \begin{bmatrix} \sum_{i=1}^{M} w_{1,i}H_i^T \\ \sum_{i=1}^{M} w_{2,i}H_i^T \\ \vdots \\ \sum_{i=1}^{M} w_{K,i}H_i^T \end{bmatrix} = \begin{bmatrix} w_{1,1} & w_{1,2} & \cdots & w_{1,M} \\ w_{2,1} & w_{2,2} & \cdots & w_{2,M} \\ \vdots & \vdots & \ddots & \vdots \\ w_{K,1} & w_{K,2} & \cdots & w_{K,M} \end{bmatrix} \begin{bmatrix} H_1^T \\ H_2^T \\ \vdots \\ H_M^T \end{bmatrix} \\
&= \mathbf{W}_{K\times M}\mathbf{H}_{M\times N_T}
\end{aligned} \quad (34)$$

In the light of (34), micro-motion signal separation can be regarded as the solution of $\mathbf{H}$ when $\mathbf{Y}$ is known. In addition, we can draw the conclusion that the basic signal of each scattering point is independent from each other according to (5), (7) and (12). Based on the observation matrix and the mutual independence of the source signal, the solution of such question is classified as blind source separation.

Blind source separation theory holds that if the source signals are mutually independent and are mixed linearly, the source signals can be reconstructed based on the observation signal [27]. As for the micro-motion signal separation in this paper, the theory means that the basic signal matrix $\mathbf{H}$ can be reconstructed by using the observation matrix $\mathbf{Y}$.

Define $\mathbf{H}'$ as the reconstructed matrix, $\mathbf{W}'$ as the unmixed matrix. The algorithm of separating micro-motion signals can be described as: using the dependence of $\mathbf{H}'$ as an indicator, find a unmixed matrix $\mathbf{W}'$, and make the reconstructed matrix $\mathbf{H}' = \mathbf{W}' \times \mathbf{Y} = \mathbf{W}' \times \mathbf{W} \times \mathbf{Y}$. $\mathbf{H}'$ is the optimal approximation of $\mathbf{H}$. The process can be summarized as

$$L(\mathbf{W}') = \min(\max) f(\mathbf{W}', \mathbf{Y}) \tag{35}$$

where $f(\mathbf{W}', \mathbf{Y})$ is the independence calculation function and $L(\mathbf{W}')$ is the independence indicator. Usually, the calculation of $\mathbf{W}'$ needs $K \geq M$, which means that the value of K should be larger than the number of the scattering point M.

Mutual information minimum, non-Gaussian maximization, negative entropy maximization and the fourth-order cumulants are the unique forms of $L(\mathbf{W}')$. Among the above, the fourth-order cumulants is one of the most effective form. At the same time, considering that the micro-motion signal processed in this paper is a complex signal, the traditional independent component analysis algorithm can not process the complex signal well. Therefore, the Joint Approximate Diagonalization of Eigen-matrices separation algorithm [28] is introduced to separate the micro-motion signals of each scattering point.

The JADE algorithm is based on the fourth-order cumulants, whose concept will be introduced as follows. Set x as a random variable, $p(x)$ as the probability density function, and the fourth-order cumulants of x can be expressed as

$$k_4 = E\left[x^4\right] - 3E\left\{\left[x^2\right]\right\}^2 \tag{36}$$

where $E[x]$ is the mathematical expectation of x.

If x is the multi-dimensional random variable, the fourth-order cumulants can be rewritten as

$$\begin{aligned} cum(x_i, x_j, x_k, x_l) = {} & E\left[x_i x_j x_k x_l\right] - E\left[x_i x_j\right] E\left[x_k x_l\right] \\ & - E\left[x_i x_k\right] E\left[x_j x_l\right] - E\left[x_i x_l\right] E\left[x_k x_j\right] \end{aligned} \tag{37}$$

The process of JADE algorithm can be summarized as follows:

Step1: centralize the observation signal of each channel in the observation matrix $\mathbf{Y}$. Set $\mathbf{Y}'$ as the centralized matrix.

$$\mathbf{Y}' = \mathbf{Y} - E(\mathbf{Y}) \tag{38}$$

Step2: find whiten matrix $\mathbf{Q}$, whiten the centralized signal $\mathbf{Y}'$ to keep the signal of every channel is not related to each other. Set the new signal matrix as $\mathbf{X}$.

$$\mathbf{X} = \mathbf{Q} \times \mathbf{Y}' \tag{39}$$

Step3: take some weight matrix, $\mathbf{M}_1, \mathbf{M}_2, \cdots, \mathbf{M}_{K_0}$, calculate the fourth-order cumulants $C_{\mathbf{X}}(\mathbf{M}_i)$ of $\mathbf{X}$ toward the weight matrix $\mathbf{M}_i$, where $i = 1, 2, \cdots, K_0$ and $K_0 = K^2$. The (p, q) element in $C_{\mathbf{X}}(\mathbf{M}_i)$ can be calculated in the following equation.

$$[C_{\mathbf{X}}(\mathbf{M}_i)]_{p,q} = \sum_{k=1}^{n} \sum_{l=1}^{n} cum(x_p, x_q, x_k, x_l) m_{k,l} \tag{40}$$

where $m_{k,l} = \mathbf{M}_i(k, l)$.

Step4: perform the joint diagonalization for $C_{\mathbf{X}}(\mathbf{M}_i)$ [29]. Calculate the unitary matrix $\mathbf{U}$ to make the criterion of the formula reach the minimum value.

$$C(\mathbf{U}) = \sum_{Mj} off\left[\mathbf{U}^H C_{\mathbf{X}}(\mathbf{M}_i) \mathbf{U}\right] \tag{41}$$

where $off(\cdot)$ represents the sum of squares of all non-diagonal elements of the solving matrix.

Step5: solve the matrix by using $\hat{\boldsymbol{W}} = \mathbf{U}^H \times \mathbf{Q}$.

Step6: estimate the source signal of each scattering point by using $\hat{\boldsymbol{H}} = \mathbf{U}^H \times \mathbf{Y} = \hat{\boldsymbol{W}} \times \mathbf{Y}$. Every row in $\hat{\boldsymbol{H}}$ represents the reconstructed basic signal.

Through the above algorithm, the basic signal fused in the echo can be separated. Although the amplitude and the order may be changed, the micro-Doppler information hidden in the phase of the basic signal will not be changed. Then, the micro-Doppler corresponding to the scattering point can be extracted through the time-frequency analysis.

C. MICRO-DOPPLER EXTRACTION

Using the algorithm mentioned above, the micro-motion signal belonging to each scattering point is separated successfully. In order to extract the micro-Doppler of the scattering point, it is necessary to use the time-frequency transform to analyze the basic signal and obtain the time-frequency graph.

The time-frequency graph obtained by time-frequency analysis has two characteristics: the first is that the amplitude of the frequency units near the real instantaneous frequency are larger than those units away from the real frequency of the signal. That is to say, the amplitude of the frequency units at any time has a characteristic of hierarchy. The second is that the real instantaneous frequency of the signal at any time is contained in the adjacent frequency units. That is to say, the real frequency is often contained in these frequency points, and its location is in the centroid position of these adjacent frequency units.

Fig. 2 is a slice of a time-frequency graph. Obviously, the values of the frequency units near the ideal frequency are larger than those away from the real frequency. The centroid position of the time-frequency graph slice is very close to the ideal frequency's position. Therefore, the position of the

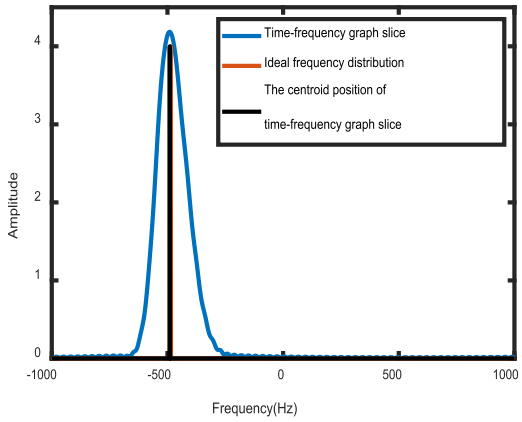

FIGURE 2. Time-frequency graph slice.

centroid can be regarded as the position of the ideal frequency, which provides a method for estimating the micro-Doppler.

Considering that the time-frequency graph often contains noise, if the micro-Doppler is extracted directly from the time-frequency graph, the extraction performance may be affected by the noise. However, as long as the impact of noise is not very serious and the position of the ideal frequency is not submerged in noise, the hierarchy characteristic will keep unchanged, which provides a method for noise reduction.

Based on the first characteristic of time-frequency graph, the amplitudes of the units near the real frequency are larger than other frequency units. In this paper, a noise reduction method for time-frequency graph based on clustering analysis is proposed. The specific process of the algorithm is as follows:

Step1: perform the short-time Fourier transform to analyze the basic signal of each scattering point, and obtain the time-frequency graph.

Step2: calculate the summation of the time-frequency graph along the column. The summation reflects the intensity of the noise at the given time. And the number of the cluster is flexibly set based on this intensity. When the noise is weak, the number of cluster can be small. On the contrary, the number of cluster can be relatively large.

Step3: according to the number of the cluster, K-Means clustering algorithm [29] is adopted to deal with these frequency units $\left[TF_{t_i,1} TF_{t_i,2} \cdots TF_{t_i,N_T}\right]$ when $t = t_i$, and the frequency units are divided into $Cluster_1$ $Cluster_2 \cdots Cluster_{K_0}$. Set the mean of different categories as $\left[ME_1\ ME_2 \cdots ME_{K_0}\right]$. Set the minimum mean as $ME_{\min}$, find the index corresponding to the category and set the index as $\mathbf{\Omega}$. Change the value of the units according to the following equation.

$$TF(f_i, t_i) = \begin{cases} 0 & f_i \in \mathbf{\Omega} \\ TF(f_i, t_i) & else \end{cases} \tag{42}$$

By employing the above clustering analysis method to denoise the time-frequency graph, the noise and redundant frequency components in the time-frequency graph are zeroed, and the clarity of the time-frequency graph is effectively improved.

After the noise reduction of the time-frequency graph, the micro-Doppler can be extracted. According to the second characteristics of the time-frequency graph, a micro-Doppler extraction algorithm based on centroid calculation is proposed in this paper. The specific process of the algorithm is as follows:

Step1: find the non-zero sequence of every column of the time-frequency graph. If the amplitude of the last frequency unit for the current unit is zero, the amplitudes of the current unit and the next unit are nonzero, the position of the current unit f_1 is labeled as the starting unit. Similarly, if the next frequency unit is zero, and the current frequency unit is nonzero, the position of the current unit f_n is labeled as the termination point.

Step2: remove the fake frequency sequence and isolated frequency sequence. According to the characteristic of the time frequency graph, set τ_0 as the threshold, the length of the continuous non-zero sequence which is less than τ_0 is set to zero. Generally, the setting of τ_0 is no more than 30.

Step3: after determining the real frequency sequence, the centroid solution method is employed to calculate the micro-Doppler of the target. Suppose that the real frequency sequence is $[f_1\ f_2\ \cdots\ f_n]$ and the values of those frequency units are $[g_1\ g_2\ \cdots\ g_n]$, the micro-Doppler f_{md} can be obtained as

$$f_{md} = \sum_{i=1}^{n} f_i \times \frac{g_i}{\sum_{i=1}^{n} g_i} \tag{43}$$

The real frequency sequence in time-frequency graph is compressed and the micro-Doppler is extracted when $t = t_i$ by using (43). Then, we perform the above operation for each moment and each scattering point, thus the micro-Doppler of the target will be extracted.

To sum up, the procedure of the micro-motion separation and micro-Doppler extraction method proposed in this paper can be concluded as follows.

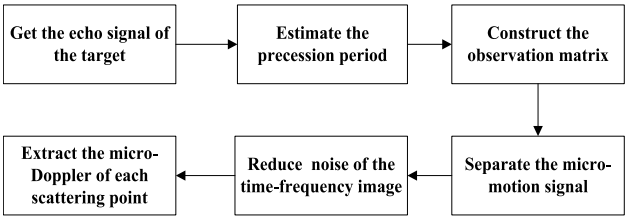

FIGURE 3. Procedure of the micro-motion signal separation and micro-Doppler estimation.

IV. SIMULATION RESULTS ANALYSIS

According to the orbital motion model in [31], the parameters are set as follows. Target launch coordinates is set to $(X_0, Y_0, Z_0) = (150 \times 10^3, 0, 0)$m, initial velocity is set to $V_k = 4 \times 10^3$m/s, and the velocity inclination is set to $\theta_k = 0.66$rad. The radar operating frequency is set to $f_c = 10$GHz,

the observation time is set to $t = 0-600$s, the pulse repetition rate is set to $PRF = 2000$Hz, and the radar observation position is set to $(X_E, Y_E, Z_E) = (0, 0, 18 \times 10^5)$m. The parameters of the target are under the following settings: $a = 0.5$m, $b = 0.02$m, $h_2 = 0.5$m, $T_c = 0.3$s, $\varepsilon = 10°$, and $\gamma \approx 14°$.

In the acquisition and processing of micro-motion signals, noise is ubiquitous and inevitable. Many papers regard noise as an important factor affecting the performance of the algorithm. The most common type of noise in signal analysis is Gaussian white noise. Therefore, this paper mainly considers the effect of noise and the type of noise is Gaussian white noise. The signal-to-noise ratio (SNR) is set to 20dB.

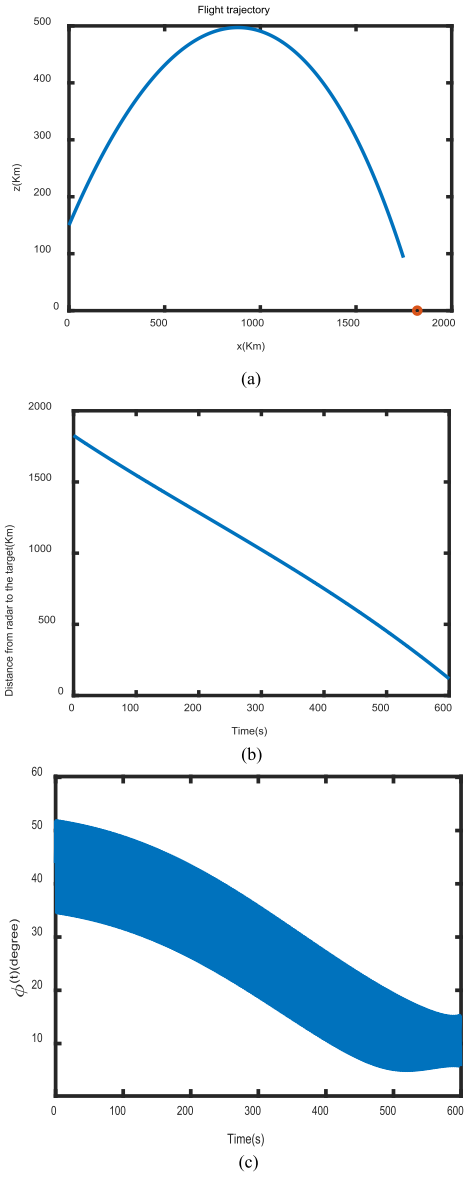

FIGURE 4. Characteristics analysis of orbit motion. (a) Flight trajectory of the target. (b) The distance between the target and the radar. (c) The change of the angle $\phi(t)$ with time.

Firstly, we analyze the characteristics of orbital motion from the simulation and the results are shown in Fig. 4.

Fig. 4(a) simulates the flight trajectory of the target, from which we can see that the orbit of the target is an elliptical orbit. Fig. 4(b) shows the distance from the target to the radar changes over time. Fig. 4(c) shows the changes of $\phi(t)$ over time. After calculation, the change of $\phi(t)$ is close to 10^{-4}rad from t to $t + T_c$. According to Fig. 4 (c), it is evident that the changes are basically the same in a relatively short observation time, which proves the basic signal of the scattering point in next period is same.

In the compensation of orbital motion in [20], the observation time is generally processed in segments, and the orbital motion is replaced by the method of polynomial equivalence. Accordingly, in the analysis of this paper, the segmentation method is also adopted to analyze the echo signal. The segmentation time is 5s. First of all, taking the echo when $t = 0 - 5$s as the observation object, the characteristic of the target is analyzed in Fig. 5.

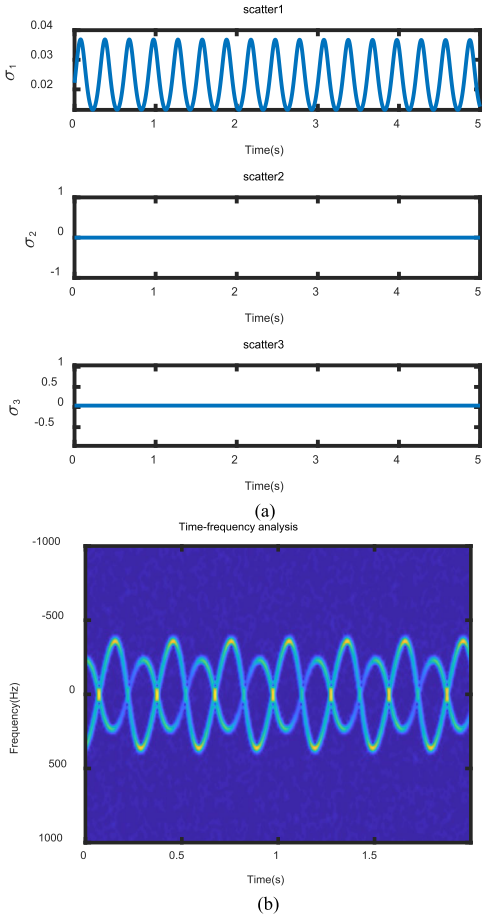

FIGURE 5. Characteristic analysis of the echo signal when $t = 0 - 5$s. (a) The change of the scattering coefficient with time. (b) The time-frequency graph of the echo signal.

Fig. 5 (a) shows the change of the scattering coefficient of each scattering point over time. The scattering coefficient of the scatter1 is approximately sinusoidal. After calculation, we find that the ratio of σ_1 in adjacent periods is a constant and the value is 1.0003, which proves that (13)

is right. The scattering coefficient of the scatter2 is 0, and the scattering coefficient of the scatter3 remains unchanged, which is consistent with (9) and (10). Fig. 5 (b) shows the time-frequency graph of the target. It can be seen from Fig 5 (b) that the micro-Doppler of the scattering points is entangled in time-frequency graph and is difficult to be extracted.

Next, the precession period needs to be estimated. Usually, the micro-motion frequency of the space target is $\omega = [2\pi\ 10\pi]$rad/s. Correspondingly, the range of N_T is from 400 to 2000. The precession period is estimated in Fig. 6.

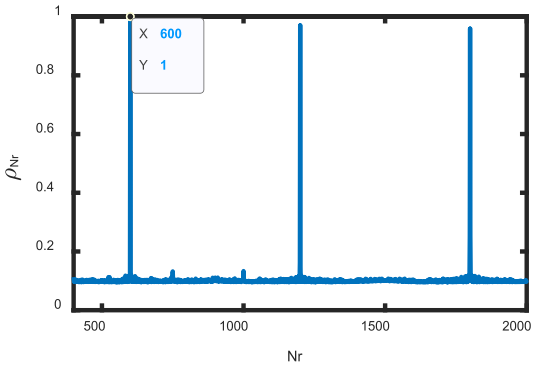

FIGURE 6. Estimation of the precession period.

Fig. 6 shows the change of the singular value ratio of the signal matrix with different lengths. It can be seen from the Fig. 6 that when $N_r = 600$, there is a peak value of ρ_{N_r}. Through calculation, it is found that the precession period estimation is $\hat{T}_c = 0.3$s which is consistent with the real target precession period.

Next, the value of K in (14) is set to 4 and the observation matrix is constructed. The micro-motion signal separation and micro-Doppler extraction results are shown in Fig. 7.

Fig. 7 (a) shows the time-frequency graph of the separated micro-motion signals. It can be seen from the Fig. 7 (a) that the basic signal belonging to each scattering point is separated effectively. However, compared with the original time-frequency graph in Fig. 5 (b), the noise in Fig. 7 (a) is further enhanced. This is because the noise is further enhanced in the process of SVD of signal matrix. Therefore, it is necessary to perform noise reduction. We use the clustering analysis to denoise the time-frequency graph. After denoising the time-frequency graph shown in Fig. 7 (a), the result is shown in Fig. 7 (b). It's obvious that the noise is removed effectively. Fig. 7 (c) and Fig. 7 (d) show the difference between the ideal micro-Doppler, the method proposed in this paper, [13], [15], IRT and Hough. Table. 1 lists the the root mean square error (RMSE) of the methods mentioned above.

Obviously, the performance of the method proposed is the best among these methods. The performance of [13] is relatively poor, and there is a wrong correlation of the scattering point. This is because [13] depends on the new interest to separate the micro-motion signal, which is likely to be invalid

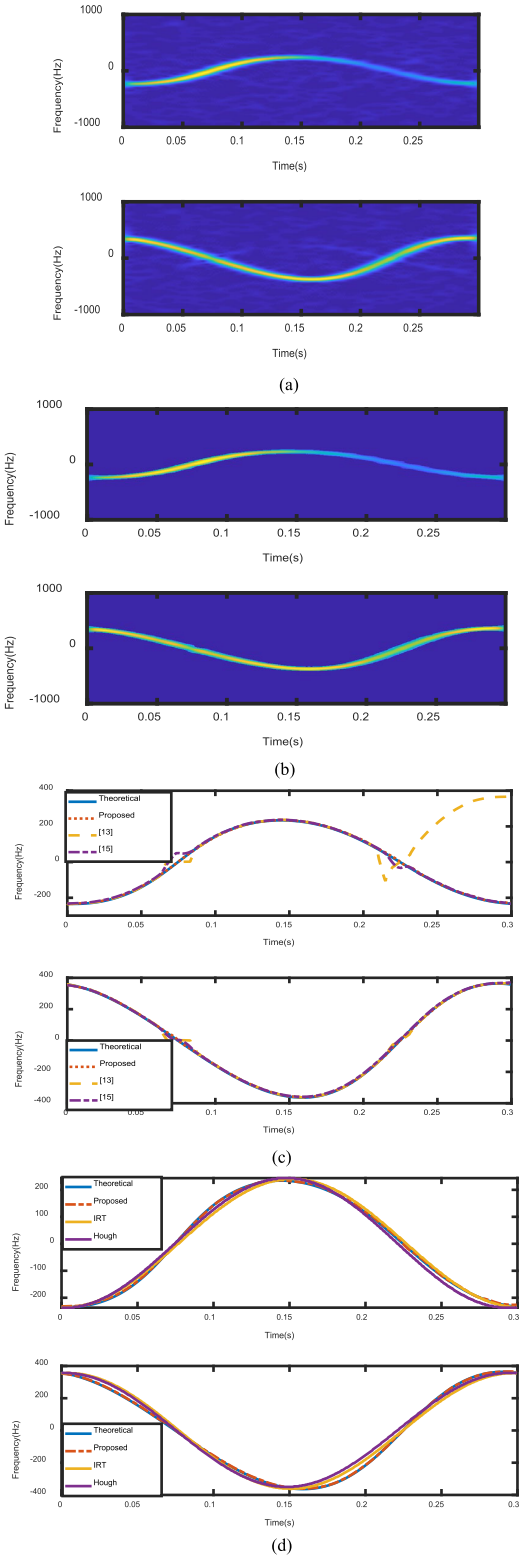

FIGURE 7. Separation of micro-motion signal and extraction of the micro-Doppler. (a) The result of the separation of the micro-motion signal. (b) The noise reduction result of the time-frequency graph. (c) Extraction results of the proposed method, [13] and [15]. (d) Extraction results of the proposed method, IRT and Hough.

at the time-frequency intersection. Although no correlation error existing in [15], there is a certain deviation at the

TABLE 1. Performance comparison of different extraction methods.

Method	Proposed	[15]	IRT	Hough	[13]
RMSE	2.61	8.39	19.58	21.25	117.31

time-frequency intersection. This is because the values of the time-frequency units at the intersection are close, which is not conductive to associate the micro-Doppler. IRT and Hough are the typical parameter estimation methods for the signals whose instantaneous frequency is sinusoidal. However, the micro-Doppler of the precession target is not strictly sinusoidal. Several parameters jointly determine the expression of the micro-Doppler. Therefore, the micro-Doppler extractions based on IRT and Hough are bad. In addition, the image processed by Hough must be a binary image. Binarization may lose some image details, which makes the performance of IRT better than Hough.

In order to further test the effectiveness of the method, the proposed method is adopted to separate signals within $t = 0 - 300$s. The observation period is divided into 60 sections, and each section is 5s. Each observation section is simulated by Monte Carlo for 50 times. Set the RMSE of the extracted micro-Doppler as the indicator. The results of the proposed method compared to [10] and [15] are shown in Fig. 8.

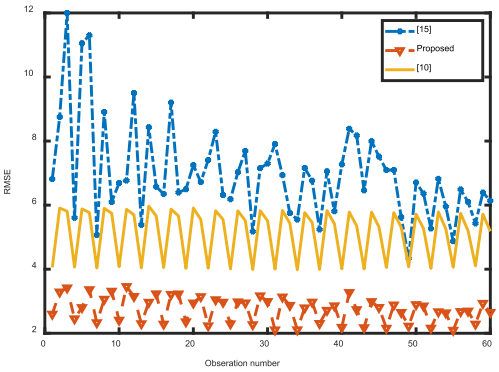

FIGURE 8. Performance of micro-Doppler extraction in different observation periods.

From Fig. 8, it is shown that the RMSE of those methods are different when the observation number is different. In addition, the variation ranges of [10] and the proposed method are smaller than [15]. All in all, the performance of the proposed method is better and more steady than [10] and [15].

In order to test the robustness of the method proposed, the simulations of the methods mentioned above is conducted under different SNR conditions.

Fig. 9 shows the performance of micro-Doppler extraction method in this paper, [10], [15] and IRT under different SNR conditions. What needs to be explained is that [10] is performed after the separation of micro-motion signal in

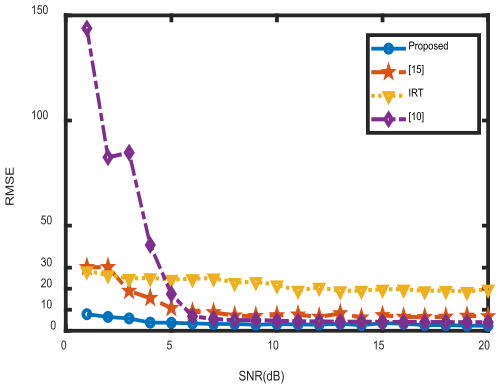

FIGURE 9. Performance of micro-Doppler extraction under different SNR.

this paper and is used to prove the advantages of the noise reduction based on clustering and micro-Doppler condensation based on centroid calculation.

Obviously, the method proposed in this paper has the best robustness among the methods above. It can be seen that when the SNR is greater than 4dB, the micro-Doppler extraction performance of the proposed method is hardly changed. When the SNR is less than 4dB, the micro-Doppler extraction performance of this algorithm gradually decreases. The extraction performance of [15] is steady when the SNR is greater than 8dB and the performance decrease when the SNR is less than 8dB. The performance of [10] is better than IRT and [15] when the SNR is greater than 6dB, but the performance degrades sharply when the SNR less than 6dB. As for the IRT, the performance declines slowly, although the RMSE is the highest when the SNR is greater than 5dB.

In the two aspects of extraction accuracy and robustness, the method in this paper is better than other similar methods. There are three reasons for the better performance of the method in this paper compared with other methods.

The first is that the proposed method is a non-parametric extraction method, in which the specific form of the signal is not required. Compared with other parametric extraction methods such as IRT, Hough and [18], the proposed method has wider application.

The second is that the proposed method adopts the idea of separating the micro-motion signals before extracting the micro-Doppler, which avoids the association errors at the time-frequency intersection. In many methods such as [13] and [15], the extraction and separation are performed simultaneously.

The third is that the noise reduction algorithm based on clustering analysis lowers the effects of the noise, which can effectively improve the robustness.

V. CONCLUSION

Space target micro-motion signal separation and micro-Doppler extraction are of great significance for space target recognition. In this paper, the cone-shaped precession target is taken as the research object. Based on the

analysis of the micro-motion and scattering characteristics, the micro-motion signal belonging to each scattering points are successfully separated by the usage of SVD and JADE. On the basis of the amplitude distribution characteristics of the time-frequency graph, the clustering analysis method is employed to reduce the noise of the time-frequency graph, and the centroid calculation method is adopted to extract the micro-Doppler. As a non-parametric extraction method, the proposed method does not require a specific form of micro-Doppler. Meanwhile, the proposed method divides the micro-Doppler extraction into two steps of signal separation and micro-Doppler extraction, which can effectively avoid micro-Doppler association errors. The simulation results show that the algorithm has good micro-Doppler extraction performance. The micro-Doppler extraction is the basis of target structure and motion feature estimation. The proposed method mainly researches on the micro-Doppler extraction, which will lay a good foundation for the estimation of target parameters and the recognition of the targets and their flying objects.

However, there are still some details that need to be improved. One is that no measured radar data are used to validate the proposed method due to the limited experimental conditions. Measured radar data are very important for verification of the method feasibility. The corresponding work will be regarded as an important point in future research. In addition, this paper only considers the detection of a single micro-motion target. Space precession targets usually appear in the form of group targets. The subsequent research will consider the micro-Doppler extraction of scattering point under the condition of multiple targets observation.

REFERENCES

[1] S. Ghio, M. Martorella, D. Staglianó, D. Petri, S. Lischi, and R. Massini, "Practical implementation of the spectrogram-inverse radon transform based algorithm for resident space objects parameter estimation," *IET Sci., Meas. Technol.*, vol. 13, no. 9, pp. 1254–1259, Nov. 2019.

[2] M. S. Andrew, M. C. John, and D. Bob, *Countermeasures A Technical Evaluation of the Operational Effectiveness of the Planned US National Missile Defense System*. Cambridge, U.K.: Union of Concerned Scienst, 2000.

[3] M. Zarei-Jalalabadi and S. M.-B. Malaek, "Motion estimation of uncooperative space objects: A case of multi-platform fusion," *Adv. Space Res.*, vol. 62, no. 9, pp. 2665–2678, Nov. 2018.

[4] D. Tahmoush, "Review of micro-Doppler signatures," *IET Radar, Sonar Navigat.*, vol. 9, no. 9, pp. 1140–1146, Dec. 2015.

[5] C. V. Chen, "Doppler signatures of radar backscattering from objects with micro-motions," *IET Signal Process.*, vol. 3, no. 2, pp. 291–300. 2008.

[6] S. A. Musa, R. S. A. R. Abdullah, A. Sali, A. Isma'il, and N. E. A. Rashid, "Low-slow-small (LSS) target detection based on micro Doppler analysis in forward scattering radar geometry," *Sensors*, vol. 19, no. 15, pp. 3332-1–3332-20, Jul. 2019.

[7] S. A. Musa, R. S. A. R. Abdullah, A. Sali, A. Isma'il, and N. E. A. Rashid, "DVBS based forward scattering radar for drone detection," in *Proc. 20th Int. Radar Symp. (IRS)*, Ulm, Germany, Jun. 2019, pp. 1–8.

[8] T. S. Murray, D. R. Mendat, K. A. Sanni, P. O. Pouliquen, and A. G. Andreou, "Bio-inspired human action recognition with a micro-Doppler sonar system," *IEEE Access*, vol. 6, pp. 28388–28403, 2018.

[9] I. Jouny, "Extraction of scattering centers for target recognition using ESPRIT," in *Proc. Int. Conf. Electromagn. Adv. Appl. (ICEAA)*, Verona, Italy , Sep. 2017, pp. 453–456.

[10] Z.-R. Chen, H. Gu, W.-M. Su, and Z. Wang, "Micro-Doppler separation from time frequency distribution based on direction pattern," in *Proc. 12th Int. Conf. Signal Process. (ICSP)*, Hangzhou, China, Oct. 2014, pp. 2116–2119.

[11] Y. Zhou, D. Bi, A. Shen, and X. Wang, "Hough transform-based large micro-motion target detection and estimation in synthetic aperture radar," *IET Radar, Sonar Navigat.*, vol. 13, no. 4, pp. 558–565, Apr. 2019.

[12] P. Sathe, A. Dyana, K. P. Ray, D. Shashikiran, and A. Vengadarajan, "Helicopter main and tail rotor blade parameter extraction using micro-Doppler," in *Proc. 19th Int. Radar Symp. (IRS)*, Bonn, Germany, Jun. 2018, pp. 1–10.

[13] X. Han, "Research on recognition of space cone-shaped targets based on narrowband radar feature," Ph.D. dissertation, Dept. Elect. Eng., Xidian Univ., Xian, Shaanxi, China, 2015.

[14] P. Li, D.-C. Wang, and L. Wang, "Separation of micro-Doppler signals based on time frequency filter and Viterbi algorithm," *Signal, Image Video Process.*, vol. 7, no. 3, pp. 593–605, May 2013.

[15] P. Li and Q. Zhang, "An improved Viterbi algorithm for IF extraction of multicomponent signals," *Signal Image Video Process.*, vol. 12, no. 1, pp. 171–179. 2018.

[16] D. P. Fairchild and R. M. Narayanan, "Classification of human motions using empirical mode decomposition of human micro-Doppler signatures," *IET Radar, Sonar Navigat.*, vol. 8, no. 5, pp. 425–434, Jun. 2014.

[17] I. Djurović, V. Popović-Bugarin, and M. Simeunović, "The STFT-Based estimator of micro-Doppler parameters," *IEEE Trans. Aerosp. Electron. Syst.*, vol. 53, no. 3, pp. 1273–1283, Jun. 2017.

[18] S. Vishwakarma and S. S. Ram, "Detection of multiple movers based on single channel source separation of their micro-Dopplers," *IEEE Trans. Aerosp. Electron. Syst.*, vol. 54, no. 1, pp. 159–169, Feb. 2018.

[19] P. Huang, H. Yin, and X. Xu, "Radar cross section of all kinds of targets," in *Radar target Characteristics*. Beijing, China: Publishing House of Electronics Industry, 2006, pp. 67–99.

[20] S. He, H. Zhao, and Y. Zhang, "Translational motion compensation for ballistic targets based on delayed conjugated multiplication," *J. Radars*, vol. 3, no. 5, pp. 505–510. 2016.

[21] W. Zhang, K. Li, and W. Jiang, "Parameter estimation of radar targets with macro-motion and micro-motion based on circular correlation coefficients," *IEEE Signal Process. Lett.*, vol. 22, no. 5, pp. 633–637, May 2015.

[22] W. Zhang, Y. Fu, and J. Yin, "Micro-Doppler period estimation based on concentration statistics of ambiguity function," *IEEE Trans. Aerosp. Electron. Syst.*, vol. 56, no. 3, pp. 1722–1741, Jun. 2020, doi: 10.1109/TAES.2019.2921192.

[23] J. J. M. de Wit, R. I. A. Harmanny, and P. Molchanov, "Radar micro-Doppler feature extraction using the singular value decomposition," in *Proc. Int. Radar Conf.*, Oct. 2014, pp. 1–6.

[24] P. Addabbo, C. Clemente, and S. L. Ullo, "Fourier independent component analysis of radar micro-Doppler features," in *Proc. IEEE Int. Workshop Metrol. Aerosp. (MetroAeroSpace)*, Padua, Italy, Jun. 2017, pp. 45–49.

[25] H. Zhu, S. Zhang, and H. Zhao, "Single-channel source separation of multi-component radar signal based on EVD and ICA," *Digit. Signal Process.*, vol. 57, pp. 93–105, Oct. 2016.

[26] M. H. Mostafa, S. Chamaani, and J. Sachs, "Singular spectrum analysis-based algorithm for vitality monitoring using M-sequence UWB sensor," *IEEE Sensors J.*, vol. 20, no. 9, pp. 4787–4802, May 2020.

[27] I. Domanov and L. D. Lathauwer, "Generic uniqueness of a structured matrix factorization and applications in blind source separation," *IEEE J. Sel. Topics Signal Process.*, vol. 10, no. 4, pp. 701–711, Jun. 2016.

[28] M. M. Hussain, Z. Zakaria, R. Rifin, M. Z. Hussin, N. H. Abdul Rahman, N. I. Ilham, N. M. Zain, and M. M. Sani, "Prediction of time series based on load profile using JADE technique," in *Proc. IEEE 8th Control Syst. Graduate Res. Colloq. (ICSGRC)*, Aug. 2017, pp. 33–36.

[29] E. M. Fadaili, N. T. Moreau, and E. Moreau, "Nonorthogonal joint diagonalization/zero diagonalization for source separation based on time-frequency distributions," *IEEE Trans. Signal Process.*, vol. 55, no. 5, pp. 1673–1687, May 2007.

[30] Z. L. Jiang, N. Guo, Y. Jin, J. Lv, Y. Wu, Z. Liu, J. Fang, S. M. Yiu, and X. Wang, "Efficient two-party privacy-preserving collaborative k-means clustering protocol supporting both storage and computation outsourcing," *Inf. Sci.*, vol. 518, pp. 168–180, May 2020.

[31] L. He, *Solid Ballistic Missile Design*. Beijing, China: Beijing Univ. Aeronaut. Astronaut. Press, 2004, pp. 1–15.

XUGUANG XU was born in Xi'an, Shaanxi, China, in 1994. He received the B.S. degree in radar engineering, in 2016, and the M.S. degree in electronic science and engineering from Air Force Engineering University, Xi'an, in 2018, respectively, where he is currently pursuing the Ph.D. degree. His research interests include micro-motion signal processing and target recognition.

CUNQIAN FENG received the Ph.D. degree from Air Force Engineering University, Xi'an, China, in 2003. He is currently a Professor with Air Force Engineering University. His research interests include radar signal processing and electronic countermeasure.

SISAN HE was born in 1981. He is currently an Associate Professor with the Air and Missile Defense College, Air Force Engineering University. His research interests include radar target recognition and nonstationary signal processing.